# Direct limits on the interaction of antiprotons with axion-like dark matter

https://doi.org/10.1038/s41586-019-1727-9

Received: 21 May 2019

Accepted: 20 September 2019

Published online: 13 November 2019

C. Smorra[1*], Y. V. Stadnik[2,3], P. E. Blessing[1,4], M. Bohman[1,5], M. J. Borchert[1,6], J. A. Devlin[1,7], S. Erlewein[1,5,7], J. A. Harrington[1,5], T. Higuchi[1,8,12], A. Mooser[1,5], G. Schneider[1,9], M. Wiesinger[1,5], E. Wursten[1,7], K. Blaum[5], Y. Matsuda[8], C. Ospelkaus[5,10], W. Quint[4], J. Walz[2,9], Y. Yamazaki[1], D. Budker[2,11] & S. Ulmer[1*]

Astrophysical observations indicate that there is roughly five times more dark matter in the Universe than ordinary baryonic matter[1], and an even larger amount of the Universe's energy content is attributed to dark energy[2]. However, the microscopic properties of these dark components remain unknown. Moreover, even ordinary matter—which accounts for five per cent of the energy density of the Universe—has yet to be understood, given that the standard model of particle physics lacks any consistent explanation for the predominance of matter over antimatter[3]. Here we present a direct search for interactions of antimatter with dark matter and place direct constraints on the interaction of ultralight axion-like particles (dark-matter candidates) with antiprotons. If antiprotons have a stronger coupling to these particles than protons do, such a matter–antimatter asymmetric coupling could provide a link between dark matter and the baryon asymmetry in the Universe. We analyse spin-flip resonance data in the frequency domain acquired with a single antiproton in a Penning trap[4] to search for spin-precession effects from ultralight axions, which have a characteristic frequency governed by the mass of the underlying particle. Our analysis constrains the axion–antiproton interaction parameter to values greater than 0.1 to 0.6 gigaelectronvolts in the mass range from $2 \times 10^{-23}$ to $4 \times 10^{-17}$ electronvolts, improving the sensitivity by up to five orders of magnitude compared with astrophysical antiproton bounds. In addition, we derive limits on six combinations of previously unconstrained Lorentz- and CPT-violating terms of the non-minimal standard model extension[5].

Various experiments aim at the detection of axions and axion-like particles to identify the microscopic nature of dark matter[6,7]. Axions are light spinless bosons (axion mass, $m_a \ll 1\ \mathrm{eV}\ c^{-2}$; $c$, speed of light), which were originally proposed to resolve the strong charge–parity (CP) problem of quantum chromodynamics[8] and were later identified as excellent dark-matter candidates. Although limits have been placed on their interaction strengths with photons, electrons, gluons and nucleons[7,9], direct information on the strength of their interaction with antimatter is lacking. In the standard model, interactions have equal couplings to conjugate fermion–antifermion pairs because the combined charge-, parity- and time-reversal (CPT) invariance is a fundamental symmetry. CPT invariance has been tested with high sensitivity in recent precision measurements on antihydrogen, antiprotonic helium and antiprotons[4,10–14]; so far, no indications of a violation have been found. By contrast, the non-observation of primordial antimatter and the matter excess in our Universe are tremendous challenges for the standard model because the tiny amount of CP violation contained in the standard model predicts eight orders of magnitude less matter content than what we actually observe[3]. However, the discovery of an asymmetric coupling of dark-matter particles to fermions and antifermions may provide an important clue and improve our understanding of dark matter and the baryon asymmetry. Such an asymmetric coupling may in principle arise for axion-like particles if the underlying theory is non-local[15]. Here we test for possible signatures of such a coupling in the spin transitions of a single antiproton.

The canonical axion and axion-like particles (collectively referred to as 'axions' hereafter) can be hypothetically produced in the early Universe by non-thermal mechanisms, such as 'vacuum misalignment'[16]. Subsequently, they form the coherently oscillating classical field $a \approx a_0 \cos(\omega_a t)$, where the angular frequency is given by $\omega_a \approx m_a c^2/\hbar$ ($\hbar$, reduced Planck constant). The axion field carries an energy density of $\rho_a \approx m_a^2 a_0^2/2$, which may comprise the entire local cold dark-matter energy density[17], $\rho_{\mathrm{DM}}^{\mathrm{local}} \approx 0.4\ \mathrm{GeV\ cm^{-3}}$. Assuming that axions account for the main part of the observed dark matter, a lower mass bound of

[1]RIKEN, Ulmer Fundamental Symmetries Laboratory, Wako, Japan. [2]Helmholtz-Institut Mainz, Johannes Gutenberg-Universität, Mainz, Germany. [3]Kavli Institute for the Physics and Mathematics of the Universe (WPI), University of Tokyo, Kashiwa, Japan. [4]GSI-Helmholtzzentrum für Schwerionenforschung GmbH, Darmstadt, Germany. [5]Max-Planck-Institut für Kernphysik, Heidelberg, Germany. [6]Institut für Quantenoptik, Leibniz Universität, Hannover, Germany. [7]CERN, Meyrin, Switzerland. [8]Graduate School of Arts and Sciences, University of Tokyo, Tokyo, Japan. [9]Institut für Physik, Johannes Gutenberg-Universität, Mainz, Germany. [10]Physikalisch-Technische Bundesanstalt, Braunschweig, Germany. [11]Department of Physics, University of California, Berkeley, CA, USA. [12]Present address: Research Center for Nuclear Physics, Osaka University, Ibaraki, Japan. *e-mail: Christian.Smorra@cern.ch; Stefan.Ulmer@cern.ch

$m_a \gtrsim 10^{-22}$ eV is imposed by the requirement that the reduced de Broglie wavelength of the axion does not exceed the size of the dark-matter halo of the smallest dwarf galaxies (about 1 kpc).

Fermions may interact with axions by a so-called derivative interaction, causing spin precession[18]. In the non-relativistic limit, the relevant part of this interaction can be described by the time-dependent Hamiltonian[18,19]:

$$H_{\mathrm{int}}(t) \approx \frac{C_{\bar{p}} a_0}{2 f_a} \sin(\omega_a t) \boldsymbol{\sigma}_{\bar{p}} \cdot \mathbf{p}_a \tag{1}$$

where $\boldsymbol{\sigma}_{\bar{p}}$, $\mathbf{p}_a$, $f_a$ and $C_{\bar{p}}$ are the Pauli spin-matrix vector of the antiproton $\bar{p}$, the momentum vector of the axion field, the axion decay constant, and a model-dependent dimensionless parameter, respectively. The ratio $C_{\bar{p}}/f_a$ is proportional to the axion–antiproton interaction strength. We note that the fundamental theory to produce a CPT-odd operator like the one in equation (1) with $C_{\bar{p}} \neq C_p$ would need to be non-local[15].

The leading-order shift of the antiproton spin-precession frequency due to the interaction in equation (1) is given by:

$$\delta\omega_L^{\bar{p}}(t) \approx \frac{C_{\bar{p}} m_a a_0 |\mathbf{v}_a|}{f_a} [A \cos(\Omega_{\mathrm{sid}} t + \alpha) + B] \sin(\omega_a t) \tag{2}$$

where $|\mathbf{v}_a| \sim 10^{-3} c$ ('~' indicates an order-of-magnitude estimate) is the average speed of Galactic axions with respect to the Sun, $\Omega_{\mathrm{sid}} \approx 7.29 \times 10^{-5}\ \mathrm{s}^{-1}$ is the sidereal angular frequency, and $\alpha \approx -25°$, $A \approx 0.63$ and $B \approx -0.26$ are parameters determined by the orientation of the experiment relative to the Galactic-axion dark-matter flux[20] (see Supplementary Information). We note that the time-dependent perturbation of the antiproton spin-precession frequency in equation (2) has three underlying angular frequencies: $\omega_1 = \omega_a$, $\omega_2 = \omega_a + \Omega_{\mathrm{sid}}$ and $\omega_3 = |\omega_a - \Omega_{\mathrm{sid}}|$; these three modes have approximately evenly distributed power for the orientation of our experiment.

The experimental data used to search for the dark-matter effect were acquired using the Penning trap system of the BASE collaboration[21] at CERN's Antiproton Decelerator. We determined the magnetic moment of the antiproton, $\mu_{\bar{p}}$, by measuring the ratio of the antiproton's Larmor frequency, $\nu_L$, to the cyclotron frequency, $\nu_c$. In a time-averaged measurement, this results directly in a measurement of $\mu_{\bar{p}}$ in units of the nuclear magneton $\mu_N$:

$$\left(\frac{\nu_L}{\nu_c}\right)_{\bar{p}} = \frac{g_{\bar{p}}}{2} = -\frac{\mu_{\bar{p}}}{\mu_N} \tag{3}$$

which can be expressed in terms of the antiproton $g$-factor, $g_{\bar{p}}$. The relevant part of the apparatus for this measurement is shown in Fig. 1. We used a multi-trap measurement scheme with two single antiprotons to determine $\mu_{\bar{p}}$ with a precision 350 times better than that of the best so far single-trap measurement[22]. Our multi-trap measurement scheme is described in detail in ref. [4].

The measurement of $\nu_L/\nu_c$ takes place in a homogeneous precision trap; see Fig. 1a. The cyclotron antiproton is used to determine the cyclotron frequency, $\nu_c \approx 29.7$ MHz, with a relative precision of a few parts per billion[13] (ppb) from the spectra of image-current signals, such as those shown in Fig. 1b. For the measurement of $\nu_L$, the cyclotron antiproton is moved by voltage ramps into the park trap, and the Larmor antiproton is shuttled into the precision trap. We drive spin transitions in the precision trap using an oscillating magnetic field with a frequency of $\nu_{\mathrm{rf}} \approx 82.85$ MHz. To observe these spin transitions, we need to identify the initial and final spin states of each spin-flip drive in the precision trap. To this end, we transport the Larmor antiproton into the analysis trap and use the continuous Stern–Gerlach effect[23], where a strong magnetic curvature of about $3 \times 10^5\ \mathrm{T\,m^{-2}}$ couples the magnetic moment of the antiproton to its axial motion. As a consequence, spin transitions become observable as an axial-frequency shift of $\Delta\nu_{z,\mathrm{SF}} \approx \pm 172$ mHz. The spatial separation of the analysis trap from the precision trap strongly reduces line broadening effects from the magnetic inhomogeneity of the analysis trap in the measurement of the frequency ratio, which is a key technique that enables precision measurements of $\mu_{\bar{p}}$ at the parts-per-billion level. The identification of the spin state in the analysis trap is performed using a sequence of axial-frequency measurements with interleaved resonant spin-flip drives, as shown in Fig. 1c. The average fidelity of the identification of spin transitions in the presence of axial-frequency fluctuations is about 80% (ref. [4]).

To determine the antiproton $g$-factor, we measure the spin-flip probability $P_{\mathrm{SF,PT}}$ as a function of the frequency ratio $\Gamma = \nu_{\mathrm{rf}}/\nu_c$ in the precision trap, which gives the antiproton spin-flip resonance shown in Fig. 1d. The data consist of 933 spin-flip experiments recorded over 85 days from 5 September 2016 to 27 November 2016. The duration of the measurement cycle of the resonance is not constant, mainly owing to the statistical nature of the spin-state readout. The median cycle frequency is about 0.38 mHz ≈ (44 min)$^{-1}$. The spin-flip drive duration is $t_{\mathrm{rf}} = 8$ s, with a constant drive amplitude for all data points. The drive frequency varies in the range ± 45 ppb (±3.7 Hz) around the expected Larmor frequency. The time-averaged value of $\mu_{\bar{p}}$ is extracted by matching the lineshape of an incoherent Rabi resonance to the data, which results in $g_{\bar{p}}/2 = 2.792\,847\,344\,1(42)$ with a relative uncertainty of 1.5 ppb (ref. [4]).

The frequency shift in equation (2) causes a time-dependent detuning of the drive and the Larmor frequency in each spin-flip experiment. In the following, we consider slow dynamic effects on spin transitions, where $\omega_a/(2\pi) \ll 1/t_{\mathrm{rf}} = 125$ mHz, so that the variation of the effective Larmor frequency is negligible during the spin-flip drive and does not affect the spin motion on the Bloch sphere. Each spin-flip experiment with a drive time of $t$ probes the 'instantaneous value' of the Larmor frequency, $\omega_L + \delta\omega_L^{\bar{p}}(t)$.

To determine whether or not an axion–antiproton coupling is observed, we perform a hypothesis test using the test statistic $q = -2\ln\lambda$, where $\lambda$ denotes the likelihood ratio (see Supplementary Information). We compare the zero-hypothesis model $H_0$ with $\delta\omega_L^{\bar{p}}(t) = 0$ with the extended models $H_b(\omega)$, which add an oscillation with frequency $\omega$ to $H_0$ and have the amplitude $b(\omega) \geq 0$ and the phase $\varphi(\omega)$ as free parameters. The test statistic is evaluated for a set of fixed frequencies with a frequency spacing of 60 nHz, which is narrower than the detection bandwidth of our measurement, about $1/T_{\mathrm{meas}} \cong 130$ nHz. In this evaluation we consider the frequency range 5 nHz ≤ $\omega/(2\pi)$ ≤ 10.49 mHz and perform a multiple-hypothesis test with $N_0 = 174{,}876$ test frequencies. The test statistic for the experimental data as a function of the test frequency is shown in Fig. 2. To define the detection thresholds, we use Wilk's theorem to obtain the distribution of the test statistic for zero-oscillation data and correct for the 'look elsewhere' effect (see Supplementary Information for details). We find that our highest value, $q_{\mathrm{max}} = 25.4$, in the entire evaluated frequency range corresponds to a local $p$ value of $p_L = 3 \times 10^{-6}$. This results in a global $p$ value of $p_G = 0.254$ for our multi-hypothesis test, which represents the probability that rejecting $H_0$ in favour of any of the alternative models $H_b(\omega)$ is wrong. Consequently, we find no statistically significant indication of a periodic interaction of the antiproton spin at the sensitivity of our measurement, and conclude that our measurement is consistent with the zero hypothesis in the tested frequency range.

To set experimental amplitude limits, we apply the $\mathrm{CL_s}$ method[24]. We first extract amplitude limits for the single-mode oscillations $b_{\mathrm{SM}}(\omega)$ with a 95% confidence level; the results are shown in Fig. 3a. In the frequency range 190 nHz ≤ $\omega/(2\pi)$ ≤ 10 mHz, the mean limit on $b_{\mathrm{SM}}$ is 5.5 ppb, which corresponds to an energy resolution of about $2 \times 10^{-24}$ GeV. At lower frequencies, $\omega/(2\pi) < 130$ nHz, we sampled only a fraction of an oscillation period. Here, we consider the reduced variation of the Larmor frequency during the measurement and marginalize the quoted limit on $b_{\mathrm{SM}}(\omega)$ over the starting phase (see Supplementary Information). To constrain the axion–antiproton coupling coefficient $f_a/C_{\bar{p}}$, we assume that the axion field has a mean energy density equal to the average local dark-matter energy density $\rho_{\mathrm{DM}}^{\mathrm{local}} \approx 0.4\ \mathrm{GeV\ cm^{-3}}$ during

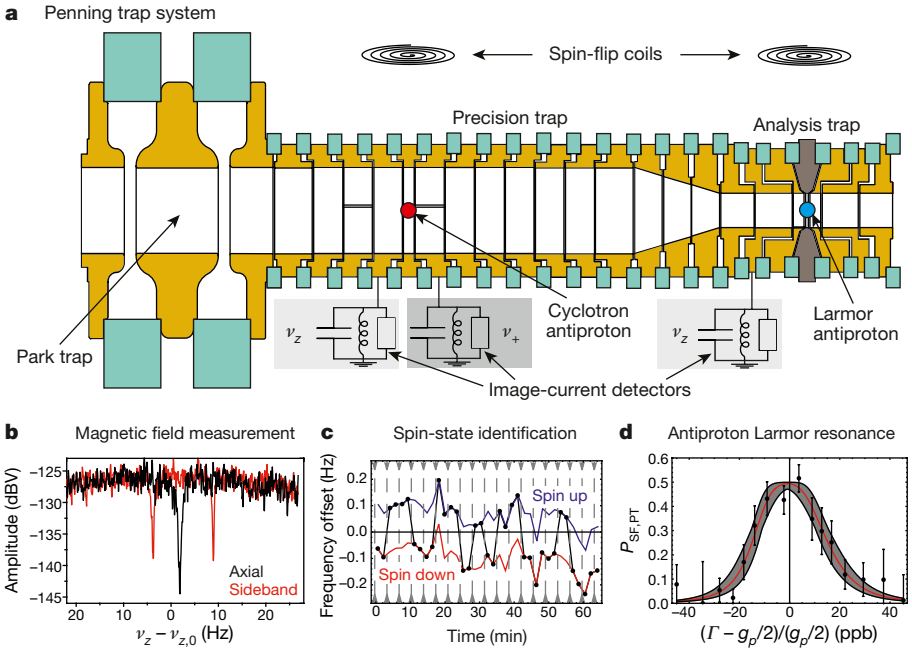


**Fig. 1 | Measurement of the magnetic moment of the antiproton. a**, The multi-Penning-trap system used for the measurement of the magnetic moment of the antiproton; shown are the cyclotron antiproton, the Larmor antiproton and three Penning traps[4]. The trap system consists of a stack of gold-plated copper and CoFe electrodes (yellow and brown, respectively) separated by sapphire rings (green). The image-current detectors used for the axial frequency $\nu_z$ and the modified cyclotron frequency $\nu_+$ are represented by the circuits in the light-gray and dark-gray boxes, respectively. **b**, Two fast Fourier transform spectra of the image-current signal of the cyclotron antiproton used to determine the axial frequency (black curve) and the cyclotron sidebands (red curve). The sideband signal is measured while coupling the axial and cyclotron modes with a quadrupolar radiofrequency drive. The cyclotron frequency $\nu_c$ in the precision trap is extracted from these two spectra[21]. **c**, A measurement sequence used for the identification of the antiproton spin state in the analysis trap. A series of axial-frequency measurements is interleaved with resonant spin-flip drives. The spin state can be assigned with high fidelity by detecting the induced axial-frequency shifts[31]. **d**, Larmor resonance of the Larmor antiproton in the precision trap, resulting from measuring the spin-flip probability $P_{SF,PT}$ in the precision trap at the normalized frequency $\Gamma = \nu_{rf}/\nu_c$. The measurement is referenced to the proton $g$-factor value from 2014[32]: $g_p/2 = 2.792847350(9)$. The error bars correspond to 1 s.d. uncertainties.

the measurement, and use equation (2) to relate $f_a/C_{\bar{p}}$ to the amplitude limits. Given that the axion–antiproton coupling would produce almost equal amplitudes at the main frequency $\omega_1$ and the sideband frequencies $\omega_{2,3}$, we place limits on the coupling coefficient considering all three detection modes (see Supplementary Information). The evaluated limits on the coupling coefficient in the mass range $2\times10^{-23}\,\mathrm{eV}\,c^{-2} < m_a < 4\times10^{-17}\,\mathrm{eV}\,c^{-2}$ are shown in Fig. 3b. The sensitivity of our measurement is mass-independent in the range $m_a \gtrsim 10^{-21}\,\mathrm{eV}\,c^{-2}$, and the amplitude limit is defined by the value of the test statistic at the evaluated mass $q(m_a)$. For $q(m_a) \approx 0$, we obtain $f_a/C_{\bar{p}} > 0.6$ GeV, which represents the most stringent limitation that we can set on the basis of our data. In the low-mass range $m_a \lesssim 10^{-21}\,\mathrm{eV}\,c^{-2}$, the amplitude limit based on the non-detection at the main frequency $\omega_1$ becomes less stringent, similar to the behaviour shown in Fig. 3a. The limits in this mass range are dominated by the sideband signals $\omega_{2,3} \approx \Omega_{sid}$, which remain in the optimal frequency range of our measurement. We also marginalize these limits over the starting phase to account for the possibility of being near a node of the axion field during a measurement (see Supplementary Information). These effects lead to less stringent limits on the coupling coefficient for low masses. We conclude that the limits on the axion–antiproton coupling coefficient range from 0.1 GeV to 0.6 GeV in the tested mass range. For comparison, the most precise matter-based laboratory bounds on the axion–nucleon ($N$) interaction in the same mass range are at the level $f_a/C_N \approx 10^4$–$10^6$ GeV (refs. [19,25]). As in the earlier matter-based studies[19,25], we do not marginalize our detection limits over possible fluctuations of the axion amplitude $a_0$. We note that preliminary investigations in a recent work[26] suggest that if such amplitude fluctuations are taken into account for sufficiently light axions, then the inferred limits may be weakened by up to an order of magnitude at 95% confidence level.

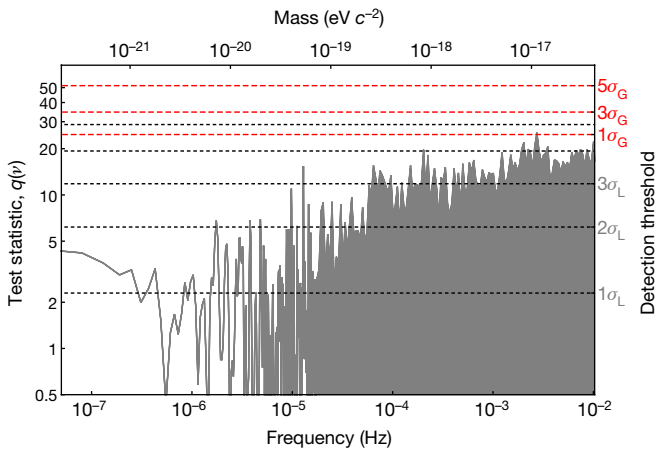


**Fig. 2 | Results of the signal detection.** The test statistic $q(\nu)$ for the experimental data as a function of the frequency $\nu$ is shown as the grey line. The red dashed lines mark the detection thresholds for the global hypothesis test and correspond to rejection errors of $1\sigma_G$ (32%), $3\sigma_G$ (0.27%) and $5\sigma_G$ ($5.7\times10^{-7}$) for the global test, where $\sigma_G$ is the standard deviation. The black dotted lines show the corresponding statistical significance $\sigma_L$ for a single local test up to $5\sigma_L$.

Our laboratory bounds are compared to astrophysical bounds in Fig. 3b. In particular, we consider the bremsstrahlung-type axion-emission process from antiprotons $\bar{p} + p \to \bar{p} + p + a$ ($p$, proton; $a$, axion) in supernova 1987A, which had a maximum core temperature of $T_{core} \approx 30$ MeV and a proton number density of $n_p \approx 5\times10^{37}\,\mathrm{cm}^{-3}$ (ref. [27]). We treat the supernova medium as being dilute (non-degenerate). In

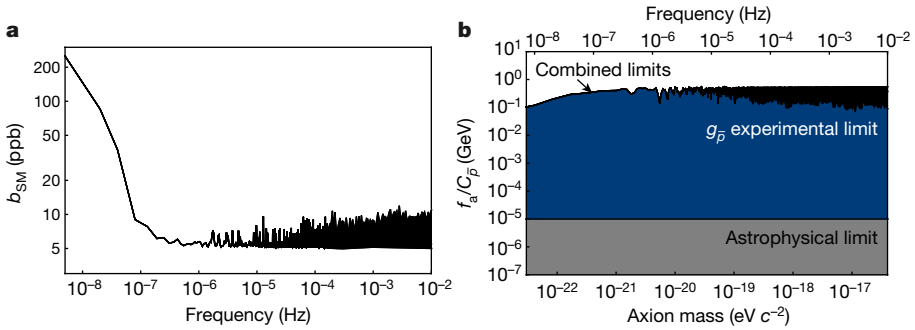


**Fig. 3 | Exclusion limits for the axion–antiproton interaction. a**, Upper 95% confidence limits on the oscillation amplitude $b_{SM}(\omega)$ of the antiproton Larmor frequency. **b**, 95% confidence limits on the axion–antiproton interaction parameter $f_a/C_{\bar{p}}$ as a function of the axion mass. The grey area shows the parameter space excluded by axion emission from antiprotons in the supernova 1987A. The dark-blue area shows the parameter space excluded from our analysis of the antiproton spin-flip data on the basis of the combined limit of the three expected oscillation modes. The black area shows the peak-to-peak difference of the upper experimental exclusion boundary of all tests within a frequency bin.

thermal equilibrium, this gives an antiproton number density of $n_{\bar{p}} \approx n_p e^{-2\xi_p/T_{core}}$, where the proton chemical potential $\xi_p$ is given by $m_p - \xi_p \approx 10$ MeV. In the limit of a dilute medium, the axion-emission rate from antiprotons scales as $\Gamma_{\bar{p}p\to\bar{p}pa} \propto n_p n_{\bar{p}} \left(C_{\bar{p}}/f_a\right)^2$, whereas the usual axion-emission rate from protons scales as $\Gamma_{pp\to ppa} \propto n_p^2 \left(C_p/f_a\right)^2$ (refs.[27,28]). Supernova bounds on the axion–proton interaction determined by considering the effect of axion emission on the duration of the observed neutrino burst vary in the range $f_a/C_p \approx 10^8$–$10^9$ GeV for $m_a \lesssim T_{core} \approx 30$ MeV, depending on the specific nuclear physics calculations employed[24,27]. Using the 'middle-ground' value and rescaling to the axion–antiproton interaction, we obtain the supernova bound $f_a/C_{\bar{p}} \gtrsim 10^{-5}$ GeV for $m_a \lesssim 30$ MeV, which is up to five orders of magnitude weaker than our laboratory bound in the relevant mass range. Indirect limits on the axion–antiproton interaction from other astrophysical sources (such as active stars and white dwarves) are even weaker because the core temperatures of such sources are much lower than those reached in supernovae.

The non-minimal standard model extension (SME) predicts an apparent oscillation of the antiproton Larmor frequency at a frequency of either $\Omega_{sid}$ or $2\Omega_{sid}$, mediated by Lorentz-violating and in some cases CPT-violating operators added to the standard model[5]. Using $P_L(\Omega_{sid}) = 0.336$ and $P_L(2\Omega_{sid}) = 0.328$, we conclude that the zero hypothesis cannot be rejected for these two frequencies, and we obtain amplitude limits of $b_{SM}(\Omega_{sid}) \le 5.3$ ppb and $b_{SM}(2\Omega_{sid}) \le 5.2$ ppb with 95% confidence level. Using these limits and the orientation of our experiment[22], we constrain six combinations of time-dependent coefficients in the non-minimal SME[5]: $\left|\tilde{b}_p^{*X}\right| < 9.7\times10^{-25}$ GeV, $\left|\tilde{b}_p^{*Y}\right| < 9.7\times10^{-25}$ GeV, $\left|\tilde{b}_{F,p}^{*XX} - \tilde{b}_{F,p}^{*YY}\right| < 5.4\times10^{-9}$ GeV$^{-1}$, $\left|\tilde{b}_{F,p}^{*(XZ)}\right| < 3.7\times10^{-9}$ GeV$^{-1}$, $\left|\tilde{b}_{F,p}^{*(YZ)}\right| < 3.7\times10^{-9}$ GeV$^{-1}$ and $\left|\tilde{b}_{F,p}^{*(XY)}\right| < 2.7\times10^{-9}$ GeV$^{-1}$, where $\tilde{b}_p^{*I}$ and $\tilde{b}_{F,p}^{*IJ}$ parameterize the perturbative energy shift of the antiproton spin levels in the non-minimal SME using the vector and tensor coefficients in the Sun-centred frame, respectively, and $I, J$ are the coordinates $X, Y, Z$ in the Sun-centred frame. These coefficients have not previously been constrained because earlier work could set limits only on effects causing a non-zero time-averaged difference of the proton and antiproton magnetic moments[4,14,22].

In conclusion, our slow-oscillation analysis of the antiproton spin-flip resonance provides limits on the coupling coefficients of the axion with an antiparticle probe. Similar searches can be performed for other antiparticles, such as positrons and anti-muons, from frequency-domain analyses of their $g$–2 measurements[29,30].

## Data availability

The datasets analysed for this study will be made available on reasonable request.

## Code availability

The analysis codes will be made available on reasonable request.

## Online content

Any methods, additional references, Nature Research reporting summaries, source data, extended data, supplementary information, acknowledgements, peer review information; details of author contributions and competing interests; and statements of data and code availability are available at https://doi.org/10.1038/s41586-019-1727-9.


1. Bertone, G., Hooper, D. & Silk, J. Particle dark matter: evidence, candidates and constraints. *Phys. Rep.* **405**, 279–390 (2005).
2. Frieman, J. A., Turner, M. S. & Huterer, D. Dark energy and the accelerating Universe. *Annu. Rev. Astron. Astrophys.* **46**, 385–432 (2008).
3. Dine, M. & Kusenko, A. Origin of the matter–antimatter asymmetry. *Rev. Mod. Phys.* **76**, 1–30 (2003).
4. Smorra, C. et al. A parts-per-billion measurement of the antiproton magnetic moment. *Nature* **550**, 371–374 (2017).
5. Ding, Y. & Kostelecky, V. A. Lorentz-violating spinor electrodynamics and Penning traps. *Phys. Rev. D* **94**, 056008 (2016).
6. Safronova, M. S., Budker, D., DeMille, D., Kimball, D. & Derevianko, A. Search for new physics with atoms and molecules. *Rev. Mod. Phys.* **90**, 025008 (2018).
7. Graham, P. W. et al. Experimental searches for the axion and axion-like particles. *Annu. Rev. Nucl. Part. Sci.* **65**, 485–514 (2015).
8. Kim, J. E. & Carosi, G. Axions and the strong CP problem. *Rev. Mod. Phys.* **82**, 557–601 (2010).
9. Stadnik, Y. V. & Flambaum, V. V. Searches for new particles including dark matter with atomic, molecular and optical systems. Preprint at https://arxiv.org/abs/1806.03115 (2018).
10. Gabrielse, G. et al. Precision mass spectroscopy of the antiproton and proton using simultaneously trapped particles. *Phys. Rev. Lett.* **82**, 3198–3201 (1999).
11. Ahmadi, M. et al. Chacterization of the 1S–2S transition in antihydrogen. *Nature* **557**, 71–75 (2018).
12. Hori, M. et al. Buffer-gas cooling of antiprotonic helium to 1.5 to 1.7 K, and antiproton-to-electron mass ratio. *Science* **354**, 610–614 (2016).
13. Ulmer, S. et al. High-precision comparison of the antiproton-to-proton charge-to-mass ratio. *Nature* **524**, 196–199 (2015).
14. Schneider, G. et al. Double-trap measurement of the proton magnetic moment at 0.3 parts per billion precision. *Science* **358**, 1081–1084 (2017).
15. Greenberg, O. W. CPT violation implies violation of Lorentz invariance. *Phys. Rev. Lett.* **89**, 231602 (2002).
16. Marsh, D. J. E. Axion cosmology. *Phys. Rep.* **643**, 1–79 (2016).
17. Catena, R. & Ullio, P. A novel determination of the local dark matter density. *J. Cosmol. Astropart. Phys.* **8**, 004 (2010).
18. Stadnik, Y. V. & Flambaum, V. V. Axion-induced effects in atoms, molecules, and nuclei: parity nonconservation, anapole moments, electric dipole moments, and spin-gravity and spin-axion momentum couplings. *Phys. Rev. D* **89**, 043522 (2014).
19. Abel, C. et al. Search for axionlike dark matter through nuclear spin precession in electric and magnetic fields. *Phys. Rev. X* **7**, 041034 (2017).
20. Legacy Archive for Microwave Background Data Analysis (LAMBDA) Tools http://lambda.gsfc.nasa.gov/toolbox/tb_coordconv.cfm (NASA/Goddard Space Flight Center, 2014).
21. Smorra, C. et al. BASE – The Baryon Antibaryon Symmetry Experiment. *Eur. Phys. J. Spec. Top.* **224**, 3055–3108 (2015).
22. Nagahama, H. et al. Sixfold improved single particle measurement of the magnetic moment of the antiproton. *Nat. Commun.* **8**, 14084 (2017).

23. Dehmelt, H. & Ekström, P. Proposed g–2/$\delta\omega_z$ experiment on single stored electron or positron. *Bull. Am. Phys. Soc.* **18**, 727–728 (1973).
24. Tanabashi, M. et al. Review of particle physics. *Phys. Rev. D* **98**, 030001 (2018).
25. Wu, T. et al. Search for axionlike dark matter with a liquid-state nuclear spin comagnetometer. *Phys. Rev. Lett.* **122**, 191302 (2019).
26. Centers, G. P. et al. Stochastic amplitude fluctuations of bosonic dark matter and revised constraints on linear couplings. Preprint at https://arxiv.org/abs/1905.13650 (2019).
27. Raffelt, G. G. in *Axions* (eds Kuster M. et al.) 51–71 (Springer, 2008).
28. Keil, W. et al. Fresh look at axions and SN 1987A. *Phys. Rev. D* **56**, 2419–2432 (1997).
29. Van Dyck, R. S., Schwinberg, P. B. & Dehmelt, H. G. New high-precision comparison of electron and positron g factors. *Phys. Rev. Lett.* **59**, 26 (1987).
30. Bennett, G. W. et al. Search for Lorentz and CPT violation effects in muon spin precession. *Phys. Rev. Lett.* **100**, 091602 (2008).
31. Smorra, C. et al. Observation of individual spin quantum transitions of a single antiproton. *Phys. Lett. B* **769**, 1 (2017).
32. Mooser, A. et al. Direct high-precision measurement of the magnetic moment of the proton. *Nature* **509**, 596 (2014).

**Acknowledgements** We acknowledge technical support by the Antiproton Decelerator group, CERN's cryolab team and all other CERN groups providing support to Antiproton Decelerator experiments. We acknowledge discussions with Y. Ding about the SME limits, and we thank A. Schwenk and K. Hebeler for sharing computing equipment for the Monte Carlo studies. We acknowledge financial support by RIKEN, MEXT, the Max Planck Society, the Max Planck–RIKEN–PTB Center for Time, Constants and Fundamental Symmetries, the European Union (Marie Skłodowska-Curie grant agreement number 721559), the Humboldt Program, the CERN fellowship programme and Helmholtz Gemeinschaft. Y.V.S. was supported by a Humboldt Research Fellowship from the Alexander von Humboldt Foundation and by the World Premier International Research Center Initiative (WPI), MEXT, Japan. D.B. acknowledges support by the DFG Reinhart Koselleck project, the ERC Dark-OsT advanced grant (project 695405), the Simons Foundation and the Heising-Simons Foundation.

**Author contributions** S.U., Y.V.S. and C.S. initiated the project. C.S. analysed the experimental data and Y.V.S. provided their theoretical interpretation and derived the constraints, which were discussed with D.B. The manuscript was written by S.U., C.S. and Y.V.S. and edited by D.B. All authors discussed and approved the manuscript.

**Competing interests** The authors declare no competing interests.

**Additional information**

**Supplementary information** is available for this paper at https://doi.org/10.1038/s41586-019-1727-9.

**Correspondence and requests for materials** should be addressed to C.S. or S.U.

**Peer review information** *Nature* thanks Gianpaolo P. Carosi and the other, anonymous, reviewer(s) for their contribution to the peer review of this work.